

High-energy gamma-ray and neutrino backgrounds from clusters of galaxies and radio constraints

Fabio Zandanel^{1,*}, Irene Tamborra¹, Stefano Gabici², and Shin'ichiro Ando¹

¹ GRAPPA Institute, University of Amsterdam, Science Park 904, 1098 XH Amsterdam, Netherlands

² APC, Univ. Paris Diderot, CNRS/IN2P3, CEA/Irfu, Obs. de Paris, Sorbonne Paris Cité, France

* e-mail: f.zandanel@uva.nl

Preprint online version: November 3, 2014

ABSTRACT

Cosmic-ray protons accumulate for cosmological times in clusters of galaxies as their typical radiative and diffusive escape times are longer than the Hubble time. Their hadronic interactions with protons of the intra-cluster medium generate secondary electrons, gamma-rays and neutrinos. In light of the high-energy neutrino events recently discovered by the IceCube neutrino observatory, for which galaxy clusters have been suggested as possible sources, and forthcoming results from the *Fermi* gamma-ray survey, we here estimate the contribution from galaxy clusters to the diffuse gamma-ray and neutrino backgrounds. We model the cluster population by means of their mass function, using a phenomenological luminosity-mass relation applied to all clusters, as well as a detailed semi-analytical model. In the latter model, we divide clusters into cool-core/non-cool-core and loud/quiet subsamples, as suggested by observations, and model the cosmic-ray proton population according to state-of-the-art hydrodynamic numerical simulations. Additionally, we consider observationally-motivated values for the cluster magnetic field. This is a crucial parameter since the observed radio counts of clusters due to synchrotron emission by secondary electrons need to be respected. For a choice of parameters respecting current constraints from radio to gamma-rays, and assuming a proton spectral index of -2 , we find that hadronic interactions in clusters contribute by less than 10% to the total extragalactic gamma-ray background observed by *Fermi* and to the IceCube flux, respectively. They account for less than 1% for spectral indices ≤ -2 . The high-energy neutrino flux observed by IceCube can be reproduced without violating radio constraints only if a very hard (and speculative) spectral index > -2 is adopted. However, this scenario is in tension with the high-energy IceCube data, which seem to suggest a spectral energy distribution of the neutrino flux that decreases with the particle energy. In the case of proton-photon interactions in clusters, we find that very likely protons do not reach sufficiently high energies to produce neutrinos in these environments. We argue that our results are optimistic due to our assumptions, and that clusters of galaxies cannot give any relevant contribution to the extragalactic gamma-ray and neutrino backgrounds. Finally, we find that the cluster contribution to the angular fluctuations in the gamma-ray background is subdominant, less than 10% at sub-degree scales.

Key words. Galaxies: clusters: general – Gamma rays: diffuse background – Gamma rays: galaxies: clusters – Neutrinos

1. Introduction

The extragalactic gamma-ray background (EGB) is the measured radiation that remains after the subtraction of all known sources from the observed gamma-ray sky. The EGB has been measured by the SAS-2 satellite for the first time (Fichtel et al. 1977), and by EGRET (Sreekumar et al. 1998; Strong et al. 2004) and *Fermi*-Large Area Telescope (LAT; Fermi-LAT Collaboration 2010b; The Fermi LAT collaboration 2014) most recently. The EGB is likely due to the sum of contributions from different unresolved sources such as active galactic nuclei (AGN), star-forming galaxies, pulsars, gamma-ray bursts, intergalactic shocks produced by structure formation, etc. (see, e.g., Dermer 2007; Abdo et al. 2010; Stecker & Venters 2011; Siegal-Gaskins et al. 2011; Ackermann et al. 2012; Fornasa et al. 2013; Di Mauro et al. 2014a,b; Tamborra et al. 2014 and references therein).

Recently the IceCube neutrino observatory at the South Pole reported evidence for extraterrestrial neutrinos (Aartsen et al. 2013, 2014b). The 4-year IceCube dataset consists of 37 events exceeding the atmospheric background with a significance of more than 5σ (Aartsen et al. 2014b). The neu-

trino data are compatible with a flux isotropically distributed in the sky, with astrophysical origin and with possible cutoff at a few PeV. The origin of these events is unknown (see Waxman 2013 and Anchordoqui et al. 2014a for recent reviews). However, the isotropic distribution in the sky of the observed events suggests that they might come from various extragalactic ~ 100 PeV cosmic-ray (CR) accelerators, such as low-power gamma-ray burst jets (Murase & Ioka 2013), AGN (Stecker 2013; Murase et al. 2014), star-forming galaxies including starbursts, galaxy mergers and AGN (Loeb & Waxman 2006; Tamborra et al. 2014; Lacki et al. 2011; Murase et al. 2013; He et al. 2013; Liu et al. 2014; Katz et al. 2013; Kashiyama & Meszaros 2014; Anchordoqui et al. 2014c; Chang & Wang 2014), intergalactic shocks and active galaxies embedded in structured regions (Murase et al. 2013). A galactic origin for the neutrinos has also been proposed (Ahlers & Murase 2014; Fox et al. 2013; Joshi et al. 2014; Taylor et al. 2014; Anchordoqui et al. 2014b) as well as mixed scenarios of galactic and extragalactic neutrino sources (Ahlers & Murase 2014; Razzaque 2013; Fox et al. 2013; Joshi et al. 2014; Murase et al. 2014; Padovani & Resconi 2014). Exotic models including PeV dark

matter decay scenarios have been discussed too (Feldstein et al. 2013; Esmaili & Serpico 2013; Esmaili et al. 2014).

As shown in Murase et al. (2013), a multi-messenger connection between the measured neutrino fluxes and their photon counterparts could be crucial to unveil the origin of the high-energy neutrinos, regardless of the physics of their sources. In the following, we will assume that the IceCube high-energy neutrinos are of extragalactic origin and are produced in proton-proton collisions. In such a scenario we would expect sources to emit also gamma-rays, at a flux comparable to that of neutrinos (see, e.g., Kelner et al. 2006). Note, however, that the neutrinos could also be produced in proton-photon interactions (see, e.g., Kelner & Aharonian 2008).

Clusters of galaxies are the latest and largest structures to form in the Universe. During their assembly, energies of the order of the gravitational binding energy, 10^{61} – 10^{63} erg, should be dissipated through structure-formation shocks and turbulence (Voit 2005). Therefore, even if only a small part of this energy goes into particle acceleration, clusters should host significant non-thermal emission from radio to gamma-rays (see, e.g., Brunetti & Jones 2014).

The contribution of clusters of galaxies to the EGB has been discussed by several authors (Loeb & Waxman 2000; Keshet et al. 2003; Gabici & Blasi 2003; Ando & Nagai 2008; Zandanel & Ando 2014). It has been argued that CR hadronic interactions in galaxy clusters could be responsible for a neutrino flux comparable to the one recently observed by IceCube (Murase et al. 2008; Kotera et al. 2009; Murase & Beacom 2013; Murase et al. 2013). However, such hadronic interactions could have a dramatic impact in the radio frequencies since secondary electrons are also produced in proton-proton interactions and radiate synchrotron emission when interacting with the magnetic fields in clusters of galaxies. The radio emission from secondary electrons needs to respect radio counts of galaxy clusters (Giovannini et al. 1999; Venturi et al. 2007, 2008; Kale et al. 2013), since the cluster diffuse synchrotron radio emission has been observed (see, e.g., Feretti et al. 2012).

In this work, we estimate possible contribution to the extragalactic gamma-ray and neutrino backgrounds from galaxy clusters assuming that gamma-rays and neutrinos mainly originate from proton-proton interactions, while taking into account for the first time the consequences in the radio regime. We compare our model estimates to the isotropic diffuse gamma-ray background measured by *Fermi* (The Fermi LAT collaboration 2014) and to the neutrino flux measured by IceCube (Aartsen et al. 2014b). We also discuss the small-scale anisotropies in EGB recently detected with *Fermi* (Fermi-LAT Collaboration 2012), and compare the measurements with cluster models. Unlike optimistic estimates in the earlier literature, we conclude that galaxy clusters cannot contribute to any of the above data substantially. This is because radio data are very constraining, almost independently of the magnetic field strength. The majority of our models predict contributions on the order of 1% or less to the isotropic components of the gamma-ray and neutrino backgrounds, while about 10% for the angular fluctuations of the EGB. If the spectral index of the accelerated protons is as hard as $E^{-1.5}$, however, it may explain much of the neutrino data, although it is a speculative case and anyhow in tension with the spectrum estimated (though with very large uncertainties) by IceCube.

This paper is organised as follows. In Section 2, we briefly discuss proton-proton interactions in galaxy clusters and explain how we calculate the emission from secondary electrons, photons and neutrinos. We then introduce the mass function of galaxy clusters and a phenomenological luminosity-mass rela-

tion in Section 3. In Section 4, we refine our approach by using a detailed semi-analytical model based on state-of-the-art numerical simulations of CRs in clusters and test the robustness of our results with respect to the adopted parameters. We briefly discuss the neutrino contribution from proton-photon interactions in clusters in Section 5, and the angular power spectrum of the EGB in Section 6. Finally, in Section 7, we summarise our findings.

2. Secondaries from proton-proton interactions

Cosmic ray protons accumulate in galaxy clusters for cosmological times (Völk et al. 1996; Berezhinsky et al. 1997) and interact with the thermal protons of the intra-cluster medium (ICM) generating secondary particles: electrons, neutrinos and high-energy photons (Dennison 1980; Blasi & Colafrancesco 1999; Miniati et al. 2001; Pfrommer & Enßlin 2004; Blasi et al. 2007; Pfrommer et al. 2008; Kushnir & Waxman 2009; Kotera et al. 2009; Pinzke & Pfrommer 2010). While the ICM density is typically well known from X-ray measurements of its bremsstrahlung emission, the CR proton spectral and spatial distributions in galaxy clusters are unknown. In fact, while the diffuse radio emission observed in several clusters proves the presence of relativistic electrons, direct proof of proton acceleration has yet to be found.

Gamma-ray constraints on the possible hadronic-induced emission started to put tight constraints on the proton content of clusters (HESS Collaboration 2009a,b; MAGIC Collaboration 2010; Fermi-LAT Collaboration 2010a; MAGIC Collaboration 2012; VERITAS Collaboration 2012; Ando & Nagai 2012; Huber et al. 2013; Vazza & Brügggen 2014; Zandanel & Ando 2014; Fermi-LAT Collaboration 2014; Prokhorov & Churazov 2014; Griffin et al. 2014). Gamma-ray limits also suggest that secondary electrons cannot be uniquely responsible for the observed radio emission in galaxy clusters, at least in the case of the so-called giant radio halos found in merging clusters like Coma (Brunetti et al. 2012; Zandanel et al. 2014b). As we will discuss in the following, an important implication for our purposes is that the observed radio counts represent an optimistic upper limit for the radio emission from secondary electrons since only a fraction of it can be of hadronic origin.

Assuming a power-law in momentum for the spectral distribution of CR protons in clusters, $f(p)dp = \rho_{\text{CR}} p^{-\alpha_p} dp$, the radio synchrotron luminosity of secondary electrons at a frequency f can be expressed as (adapted from Pfrommer et al. 2008)

$$L_f = A_f \int \rho_{\text{CR}} \rho_{\text{ICM}} \frac{\epsilon_B}{\epsilon_B + \epsilon_{\text{CMB}}} \left(\frac{\epsilon_B}{\epsilon_{B_c}} \right)^{\frac{\alpha_p - 2}{4}} dV, \quad (1)$$

where ρ_{CR} and ρ_{ICM} are respectively the CR proton and ICM density distributions, while $\epsilon_B = B^2/8\pi$ and ϵ_{CMB} are the energy densities of the cluster magnetic fields and the cosmic microwave background (CMB),¹ respectively. The parameter ϵ_{B_c} is the magnetic energy density corresponding to a characteristic magnetic field $B_c = 31(\nu/\text{GHz}) \mu\text{G}$ for the synchrotron mechanism, while A_f encloses the spectral information (Pfrommer et al. 2008). The gamma-ray luminosity of secondary photons at an energy E is defined as

$$L_\gamma = A_\gamma \int \rho_{\text{CR}} \rho_{\text{ICM}} dV, \quad (2)$$

¹ The total energy density of photons should also include the contribution from star light: $\epsilon_{ph} = \epsilon_{\text{stars}} + \epsilon_{\text{CMB}}$. However, ϵ_{stars} is subdominant in the cluster volume (see, e.g., Figure 5 of Pinzke et al. 2011) and, therefore, $\epsilon_{ph} \approx \epsilon_{\text{CMB}}$.

with A_γ enclosing the spectral information (Pfrommer et al. 2008).

In the following, we will make use of Equations (1) and (2) to calculate the hadronic-induced emission in galaxy clusters at radio and gamma-ray frequencies. The spectral multipliers A_f and A_γ were obtained in Pfrommer & Enßlin (2004) as analytical approximations of full proton-proton interaction simulations. The analytical expressions for A_f and A_γ well reproduce the results of numerical simulations from energies around the pion bump (~ 100 MeV) up to a few hundred GeV. A more precise formalism has been derived by Kelner et al. (2006) for the TeV–PeV energy range, relevant to calculate the neutrino fluxes. Therefore, we correct the gamma-ray spectra obtained adopting the analytical approximations with the recipe in Kelner et al. (2006) for energies above ~ 0.1 –1 TeV. The transition energy between the two approximations is dependent on α_p and it has been chosen as the energy at which the two models coincide.

We compute the corresponding neutrino spectra as prescribed in Kelner et al. (2006). Note that, assuming that proton-proton interactions are the main interactions producing neutrinos and gamma-rays, the neutrino intensity for all flavours could also be approximately obtained as a function of the gamma-ray flux (Ahlers & Murase 2014; Anchordoqui et al. 2004): $L_\nu(E_\nu) \approx 6 L_\gamma(E_\gamma)$, with $E_\nu \approx E_\gamma/2$, where we ignored the absorption during the propagation of gamma-rays for simplicity. From this approximation, one gets that, at a given energy, $L_\nu/L_\gamma \sim 1.5$ for $\alpha_p = 2$. However, detailed calculations by Berezhinsky et al. (1997) and Kelner et al. (2006) show that this ratio is slightly smaller for spectral indices $\alpha_p > 2$ and slightly higher for $\alpha_p < 2$.

Note that we do not assume any CR spectral cut-off at high-energies, nor any spectral steepening due to the high-energy protons that are no longer confined into the cluster (Völk et al. 1996; Berezhinsky et al. 1997; Pinzke & Pfrommer 2010), and thus, as discussed in the following, our results should be considered as conservative. While this is not relevant when comparing with the *Fermi* data, it might be relevant for the high-energy neutrino flux.

Since the larger contribution to the total diffuse intensity comes from nearby galaxy clusters (see Figure 5 and comments therein), we will additionally neglect the absorption of high-energy gamma-rays due to interactions with the extragalactic background light as this becomes relevant only at high redshifts (see, e.g., Domínguez et al. 2011). We remark that our conclusions do not change even relaxing any of the above approximations.

3. Phenomenological luminosity-mass relation

In this section, we estimate the maximum possible contribution to the extragalactic gamma-ray and neutrino backgrounds from hadronic interactions in galaxy clusters using a simplified phenomenological approach for the luminosity-mass relation.

3.1. Modelling of the diffuse gamma-ray intensity

The total gamma-ray intensity, from all galaxy clusters in the Universe, at a given energy, is

$$I_\gamma = \int_{z_1}^{z_2} \int_{M_{500,\text{lim}}} \frac{L_\gamma(M_{500}, z) (1+z)^2}{4\pi D_L(z)^2} \times \frac{d^2 n(M_{500}, z) dV_c}{dV_c dM_{500}} dz dM_{500}, \quad (3)$$

where the cluster mass M_Δ is defined with respect to a density that is $\Delta = 500$ times the *critical* density of the Universe at redshift z . V_c is the comoving volume, $D_L(z)$ is the luminosity distance, and $d^2 n(M_{500}, z)/dV_c dM_{500}$ is the cluster mass function for which we make use of the Tinker et al. (2008) formalism and the Murray et al. (2013) on-line application. The lower limit of the mass integration has been chosen to be $M_{500,\text{lim}} = 10^{13.8} h^{-1} M_\odot$, to account for large galaxy groups. The redshift integration goes from $z_1 = 0.01$, where the closest galaxy clusters are located, up to $z_2 = 2$. Where not otherwise specified, we assume $\Omega_m = 0.27$, $\Omega_\Lambda = 0.73$ and the Hubble parameter $H_0 = 100 h_{70} \text{ km s}^{-1} \text{ Mpc}^{-1}$ with $h_{70} = 0.7$. Note that where we explicitly use h in the units, as for $M_{500,\text{lim}}$, we assume $H_0 = 100 h \text{ km s}^{-1} \text{ Mpc}^{-1}$ with $h = 1$. As shown in Figure 1 (and later in Figure 5), our conclusions are not affected by the specific choice of z_2 and $M_{500,\text{lim}}$.

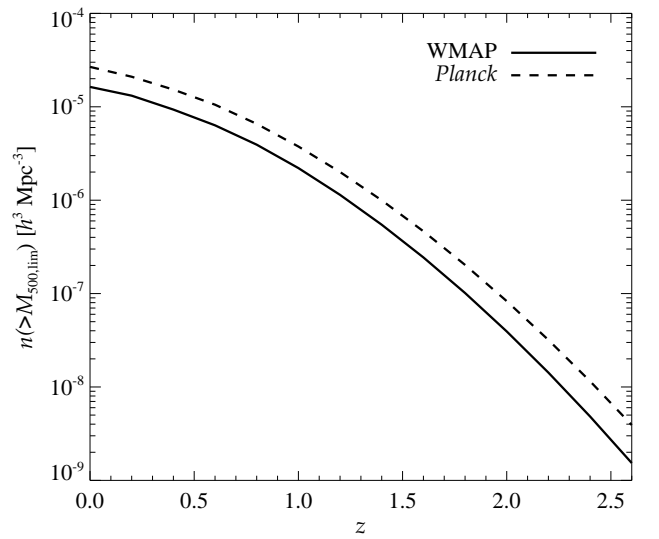


Fig. 1. Total number density of galaxy clusters for masses above $M_{500,\text{lim}} = 10^{13.8} h^{-1} M_\odot$ as a function of redshift. We show the number density obtained assuming the WMAP (Komatsu et al. 2011), our standard choice if not otherwise specified, and the *Planck* (Planck Collaboration 2013) cosmological data. At redshift $z = 2$, the number density is already negligible with respect to the lowest redshift.

We calculate the total number of detectable galaxy clusters at $f = 1.4$ GHz, above the flux F_{min} , in the following way:

$$N_{1.4}(> F_{\text{min}}) = \int_{z_1}^{z_2} \int_{F_{\text{min}}}^{\infty} \frac{d^2 n(F_{1.4}, z) dV_c}{dV_c dF_{1.4}} \frac{dV_c}{dz} dz dF_{1.4}, \quad (4)$$

where $F_{1.4} = L_{1.4}(1+z)/4\pi D_L(z)^2$, and we compare it with the radio counts from the National Radio Astronomy Observatory Very Large Array sky survey (NVSS) of Giovannini et al. (1999).² The flux F_{min} is defined as in equation (9) of Cassano et al. (2012) by adopting a noise level multiplier $\xi_1 = 1$,

² We use the cumulative number density function as in Cassano et al. (2010). Note that Cassano et al. (2010) do not use the fluxes of Giovannini et al. (1999), but the ones from follow-up observations of the same sample of galaxy clusters, which are higher than the NVSS ones (R. Cassano, private communication).

which is appropriate, while slightly optimistic, for the low redshifts of the NVSS survey ($0.44 \leq z \leq 0.2$), and a typical radio half-light radius of $R_{500}/4$ (Zandanel et al. 2014b).

The function $d^2n(F_{1.4}, z)/dV_c dF_{1.4}$ is obtained numerically from $d^2n(M_{500}, z)/dV_c dM_{500}$ by calculating $L_{1.4}(M_{500})$ from $L_\gamma(M_{500})$ as explained in the following. We here introduce a phenomenologically-driven gamma-ray luminosity-mass relation:

$$\log_{10} \left[\frac{L_\gamma(100 \text{ MeV})}{\text{s}^{-1} \text{ GeV}^{-1}} \right] = P_1 + P_2 \log_{10} \left(\frac{M_{500}}{M_\odot} \right), \quad (5)$$

where we neglect the possible redshift-dependence for simplicity.³ The radio luminosity can be obtained from the gamma-ray one by Equations (1) and (2).

In this Section we assume that the magnetic field is independent of the radius in the radio-emitting region. Therefore, the relation between radio and gamma-ray luminosities becomes

$$\frac{L_\gamma}{L_f} = \frac{A_\gamma \epsilon_B + \epsilon_{\text{CMB}}}{A_f \epsilon_B} \left(\frac{\epsilon_{Bc}}{\epsilon_B} \right)^{\frac{\alpha_p - 2}{4}}. \quad (6)$$

A special limit can be obtained for $B \gg B_{\text{CMB}}$ in all the radio-emitting region. In this case, under the hypothesis that electrons lose all their energy through synchrotron emission and $\alpha_p \approx 2$, the relation between radio and gamma-ray luminosities becomes (Pfrommer 2008):

$$\frac{L_\gamma}{L_f} \approx \frac{A_\gamma}{A_f}. \quad (7)$$

Concerning the choice of the parameters in Equation (5), we need to consider that P_1 , P_2 , α_p , B and the fraction of loud clusters are degenerate when one tries to find the maximum allowed hadronic-induced emission. The concept of loud fraction comes from the fact that, even if clusters have the same X-ray luminosity and therefore the same mass, some of them host radio emission, but others do not show any sign of it with upper limits about an order of magnitude below the loud-state. This is known as the radio–X-ray bimodality (Brunetti et al. 2009; Cassano et al. 2013). The most recent estimates suggest that the radio-loud fraction is about 20–30% (Kale et al. 2013). The subdivision of the cluster population in radio-loud and radio-quiet clusters also reflects in the corresponding gamma-ray and neutrino fluxes. Therefore, from now on we will refer to the two populations as “loud” and “quiet.” In order to obtain conservative results, in this section we will mainly consider the over-optimistic case of 100% loud clusters, and show for one choice of α_p the corresponding results for 30% of loud clusters. In the following, in order to reduce the number of free parameters, we fix $P_2 = 5/3 \approx 1.67$, i.e. we assume that the hadronic-induced luminosity scales as the cluster thermal energy $E_{\text{th}} \propto M^2/R_{\text{vir}} \propto M^{5/3}$, where R_{vir} is the virial radius. Note that the chosen P_2 parameter roughly corresponds to what is found using the Zandanel et al. (2014a) multi-frequency mock cluster catalogue (Riebe et al. 2013) for $L_\gamma(100 \text{ MeV})-M_{500}$, which typically lies in the range $\sim 1.5-1.65$ for different redshifts and different cluster populations (loud, quiet, cool-core, non cool-core). The parameter P_1 is set free to vary under the constraint that it should respect the radio counts from the NVSS survey and

³ As the larger contribution to both the number of detectable clusters in radio (Zandanel et al. 2014b) and the total gamma-ray and neutrino fluxes is dominated by nearby clusters, the high-redshift dependence is negligible for our purposes (see Section 3.2 and Figure 5 for more details).

current gamma-ray upper limits. We note that, once the thermal content of a cluster is known, the parameter P_1 could be seen as the efficiency of how much energy goes into CR acceleration.

We consider the Coma and Perseus cases for comparison with current gamma-ray upper limits on individual galaxy clusters. We take as reference the Coma upper limit obtained from 5-years of *Fermi* data by Zandanel & Ando (2014). We adopt their result for the disk model, a uniform filling of the cluster up to R_{200} , which is $F_{\text{UL}}(> 100 \text{ MeV}) = 2.9 \times 10^{-9} \text{ cm}^{-2} \text{ s}^{-1}$, obtained for a spectral index of 2. For Perseus, we assume as reference the upper limit obtained by the MAGIC Collaboration (2012) for the inner region of 0°15, which is $F_{\text{UL}}(> 1 \text{ TeV}) = 1.4 \times 10^{-13} \text{ cm}^{-2} \text{ s}^{-1}$, obtained for a spectral index of 2.2. We refer the reader to, e.g., table 1 of Huber et al. (2013) and table 2 of MAGIC Collaboration (2010) for hints on how much the gamma-ray upper limits change when modifying the spectral index. Such a change is quantifiable within a factor of about two, which does not impact our conclusions, as we will discuss later.

3.2. Results: gamma-ray and neutrino backgrounds

We assume the spectral index $\alpha_p = 2, 2.2, 2.4$, and as extreme case $\alpha_p = 1.5$, and as for the magnetic field $B \gg B_{\text{CMB}}$ (see Equation 7), $B = 1 \mu\text{G}$ and $0.5 \mu\text{G}$ (see Equation 6). The first choice of the magnetic field can be regarded as conservative considering that, for example, the volume-average magnetic field of Coma, the best studied cluster regarding Faraday rotation measurements, is of about $2 \mu\text{G}$ (Bonafede et al. 2010); the latter should be considered unrealistically optimistic with respect to current estimates. In order to clarify the meaning of the terms conservative/optimistic, note that the higher the magnetic field, the less the room for protons, as the radio counts have to be respected, and, therefore, the lower the gamma-ray and neutrino fluxes.

For each α_p and value of the magnetic field, the corresponding P_1 parameter is chosen in such a way that the computed $N_{1.4}(> F_{\text{min}})$ does not overshoot the NVSS radio counts, and is reported in Table 1. In order to make sure that our models respect current gamma-ray upper limits, the corresponding Coma-like and Perseus-like gamma-ray fluxes above 100 MeV and 1 TeV, respectively, are also shown in Table 1, assuming M_{500} as in Reiprich & Böhringer (2002), together with the total gamma-ray and neutrino flux at 100 MeV and 250 TeV, respectively, for all the galaxy clusters in the Universe. All the reported values refer to the case of 100% of loud clusters, while the case of 30% of loud clusters is studied only for $\alpha_p = 2$ (the remaining fraction of 70% quiet clusters is assumed to have a $L_\gamma(100 \text{ MeV})$ one order of magnitude lower than the loud ones).

In the last column of Table 1 and for $\alpha_p \geq 2$, we mark with “G” the cases that do not respect the gamma-ray upper limits on either Coma or Perseus. For these cases, we recompute P_1 in such a way to respect the *Coma* upper limit, our reference choice (see values in parenthesis in Table 1). However, our recomputed values for $\alpha_p = 2$ still overshoot the current Perseus gamma-ray upper limit. We nevertheless adopt the Coma upper limit as reference as it has been calculated for $\alpha_p = 2$ and for a larger spatial extension, up to R_{200} . For $\alpha_p = 1.5$, the cases marked by “N” in Table 1 exceed the IceCube neutrino data. Also in the latter case we recalculate P_1 to match the IceCube results averaging over the corresponding energy range.

Figure 2 shows both the comparison of our models to the radio counts (on the left) and the computed gamma-ray (in black) and neutrino intensities (in red) as functions of the en-

Table 1. Tested parameters and total gamma-ray and neutrino fluxes for the phenomenological luminosity-mass relation.

α_p	Loud [%]	B [μG]	P_1	Coma (> 100 MeV)	Perseus (> 1 TeV)	I_γ (100 MeV)	I_ν (250 TeV)	Notes
1.5	100	$\gg B_{\text{CMB}}$	18.60 (18.35)	$1.6 (0.92) \times 10^{-11}$	$1.7 (0.92) \times 10^{-13}$	$3.8 (2.1) \times 10^{-10}$	$7.3 (4.2) \times 10^{-19}$	N
		1	19.41 (18.35)	$1.1 (0.09) \times 10^{-10}$	$1.1 (0.09) \times 10^{-12}$	$2.5 (0.2) \times 10^{-9}$	$4.7 (0.4) \times 10^{-18}$	N
		0.5	19.91 (18.35)	$3.3 (0.09) \times 10^{-10}$	$3.4 (0.09) \times 10^{-12}$	$7.8 (0.2) \times 10^{-9}$	$1.5 (0.04) \times 10^{-17}$	N
2	100	$\gg B_{\text{CMB}}$	19.42	6.0×10^{-11}	1.1×10^{-14}	2.5×10^{-9}	4.7×10^{-21}	
		1	20.65	1.0×10^{-9}	1.8×10^{-13}	4.3×10^{-8}	8.1×10^{-20}	
		0.5	21.23 (21.09)	$3.9 (2.8) \times 10^{-9}$	$6.9 (5.0) \times 10^{-13}$	$1.6 (1.2) \times 10^{-7}$	$3.1 (2.2) \times 10^{-19}$	G
2	30	$\gg B_{\text{CMB}}$	19.60	9.1×10^{-11}	1.6×10^{-14}	1.4×10^{-9}	2.8×10^{-21}	
		1	20.82	1.5×10^{-9}	2.7×10^{-13}	2.3×10^{-8}	4.6×10^{-20}	
		0.5	21.40 (21.09)	$5.7 (2.8) \times 10^{-9}$	$1.0 (0.5) \times 10^{-12}$	$8.9 (4.4) \times 10^{-8}$	$1.8 (0.9) \times 10^{-19}$	G
2.2	100	$\gg B_{\text{CMB}}$	19.71	1.0×10^{-10}	3.6×10^{-15}	4.9×10^{-9}	5.9×10^{-22}	
		1	21.10	2.6×10^{-9}	8.7×10^{-14}	1.2×10^{-7}	1.4×10^{-20}	
		0.5	21.71 (21.16)	$1.0 (0.3) \times 10^{-8}$	$3.6 (1.0) \times 10^{-13}$	$4.9 (1.4) \times 10^{-7}$	$5.9 (1.7) \times 10^{-20}$	G
2.4	100	$\gg B_{\text{CMB}}$	19.98	1.6×10^{-10}	1.2×10^{-15}	9.1×10^{-9}	7.0×10^{-23}	
		1	21.54 (21.21)	$5.9 (2.8) \times 10^{-9}$	$4.2 (1.9) \times 10^{-14}$	$3.3 (1.6) \times 10^{-7}$	$2.5 (1.2) \times 10^{-21}$	G
		0.5	22.18 (21.21)	$2.6 (0.3) \times 10^{-8}$	$1.8 (0.2) \times 10^{-13}$	$1.4 (0.2) \times 10^{-6}$	$1.1 (0.1) \times 10^{-20}$	G

Note. For each α_p and magnetic field, the P_1 parameter of the $L_\gamma(100 \text{ MeV})-M_{500}$ obtained by taking into account the NVSS radio counts is reported in the fourth column. The fifth and sixth columns show the corresponding Coma-like and Perseus-like gamma-ray flux in $\text{cm}^{-2} \text{s}^{-1}$, respectively, integrated above 100 MeV and 1 TeV, assuming the clusters M_{500} as in Reiprich & Böhringer (2002). The seventh and eighth columns show the total gamma-ray and neutrino (all flavours) intensity at 100 MeV and 250 TeV, respectively, in $\text{cm}^{-2} \text{s}^{-1} \text{GeV}^{-1} \text{sr}^{-1}$ for all the galaxy clusters in the Universe. In the last column, we mark with ‘‘G’’ and ‘‘N’’ the cases overshooting present gamma-ray and neutrino constraints, respectively. For $\alpha_p \geq 2$, we report in parenthesis the values respecting the gamma-ray upper limit on Coma, while for $\alpha_p = 1.5$ we report in parenthesis the values matching the IceCube neutrino data averaging in the corresponding energy range. Clearly, the latter are the same in the three different magnetic field cases.

ergy (on the right), for the chosen values of α_p and B assuming 100% loud clusters. For comparison, we plot the *Fermi* data (The Fermi LAT collaboration 2014) and the IceCube 1σ error band as in Aartsen et al. (2014b). Note that the latter refers to the 4-year IceCube data sample. However, more recently a new fit has been provided, using 2-year statistics but including low energy events down to 1 TeV. The best fit of the neutrino spectrum obtained in this case scales as $E_\nu^{-2.46}$ (Aartsen et al. 2014a).

For $\alpha_p > 2$, both the gamma-ray and the neutrino diffuse backgrounds are well below the *Fermi* and the IceCube data in all cases. In the case of $\alpha_p = 2$, while the gamma-ray flux is always lower than the *Fermi* measurements, the neutrino diffuse background could represent a significant fraction of the flux measured by IceCube for $B = 1 \mu\text{G}$ and $0.5 \mu\text{G}$.

As known from radio observations, the case of 100% loud clusters is not realistic. Therefore, in Figure 3, we show the same as in Figure 2 for $\alpha_p = 2$ together with the more realistic case of 30% loud clusters. In the latter case, galaxy clusters could make up at most about 10% (20%) of the neutrino flux measured by IceCube for $B = 1 \mu\text{G}$ ($0.5 \mu\text{G}$).

In the extreme case of $\alpha_p = 1.5$, we could explain the IceCube data, averaging over the corresponding energies for all cases, while respecting all other constraints from radio to gamma-rays. However, we note that such a hard spectral index is in tension with the most recent IceCube results suggesting a softer spectral index (Aartsen et al. 2014a).

Estimates of magnetic fields in clusters from Faraday rotation measurements range from $\sim \mu\text{G}$ for merging clusters up to $10 \mu\text{G}$ for cool-core clusters (Carilli & Taylor 2002; Clarke 2004; Vogt & Enßlin 2005; Bonafede et al. 2010, 2013). The case of $B = 0.5 \mu\text{G}$ is, therefore, to be considered illustrative and optimistic as it is in tension with current knowledge.

In Equation 5 the redshift dependence has been neglected. For sake of completeness, we tested the effect of introducing a

redshift dependence in the gamma-ray luminosity-mass relation by adopting $L_\gamma \propto \Omega_m(1+z)^3 + \Omega_\Lambda$, for $\alpha_p = 2.2$, 100% loud clusters and $B \gg B_{\text{CMB}}$, roughly corresponding to the scaling observed in the Zandanel et al. (2014a) multi-frequency mock cluster catalogue (Riebe et al. 2013) for $L_\gamma(100 \text{ MeV})-M_{500}$. We found that neglecting the redshift evolution causes both the radio counts and the high-energy fluxes to be only about 20% lower than the redshift-evolution case.

We conclude that, among all the studied cases that respect at the same time radio counts and current gamma-ray upper limits, hadronic interactions in galaxy clusters realistically can contribute at most up to 10% of the total extragalactic neutrino background, while contributing less than few percents to the total extragalactic gamma-ray background. Moreover, the simplified requirement of not overshooting the NVSS radio counts on clusters results in overall optimistic results. In fact, as explained in Section 2, not all the observed radio emission in clusters has hadronic origin (Brunetti et al. 2012; Zandanel et al. 2014b). The open question is to determine the exact contribution of protons to the non-thermal content of clusters, the corresponding contribution to the observed radio emission and, therefore, the possible gamma-ray emission (see Zandanel & Ando 2014 for a discussion). This implies that even our results respecting both NVSS counts and gamma-ray limits should still be considered rather optimistic.

Finally, we note that, due to our simplified approach of a gamma-ray luminosity-mass relation, the conclusions of this section can be generalised to any source of CR protons hadronically interacting with the ICM of galaxy clusters, such as injected by structure formation shocks, AGNs, etc. For any considered source of protons, the resulting secondary emission must respect both radio and gamma-ray constraints.

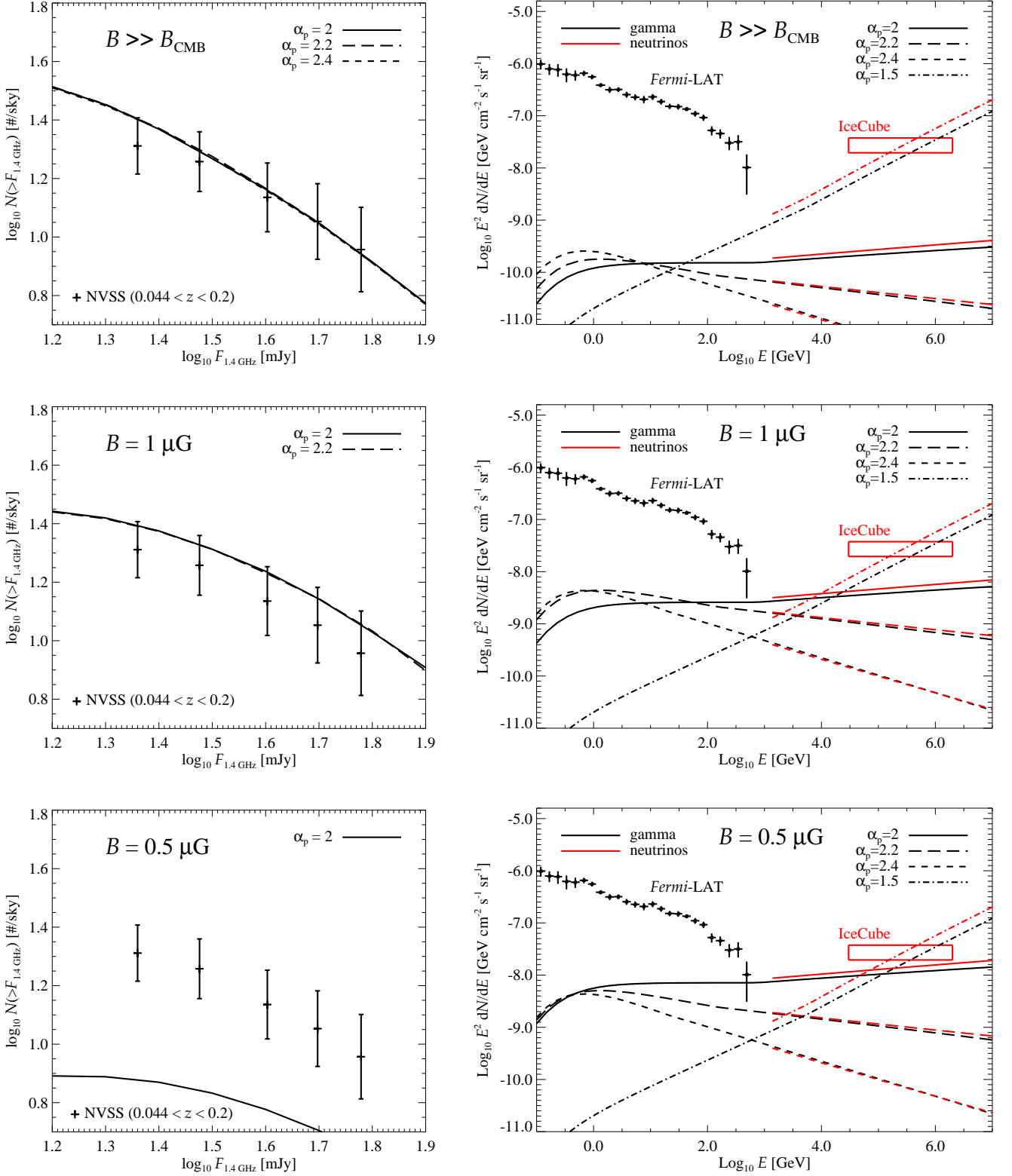


Fig. 2. Total gamma-ray and neutrino intensities (right) due to hadronic interactions in galaxy clusters, for 100% of loud clusters, and corresponding radio counts due to synchrotron emission from secondary electrons (left). From top to bottom, we plot the cases with $B \gg B_{\text{CMB}}$, $B = 1 \mu\text{G}$ and $0.5 \mu\text{G}$, respectively. For comparison, the *Fermi* (The Fermi LAT collaboration 2014) and IceCube (Aartsen et al. 2014b) data are shown in the panels on the right. The neutrino intensity is meant for all flavours. All the plotted intensities respect NVSS radio counts and the gamma-ray upper limits on individual clusters. In the case with $B = 1 \mu\text{G}$ and $\alpha_p = 2.4$, $B = 0.5 \mu\text{G}$ and $\alpha_p = 2.2, 2.4$, and for $\alpha_p = 1.5$, the radio counts respecting the gamma-ray and neutrino limits, respectively, are below the y-scale range adopted for the panels on the left.

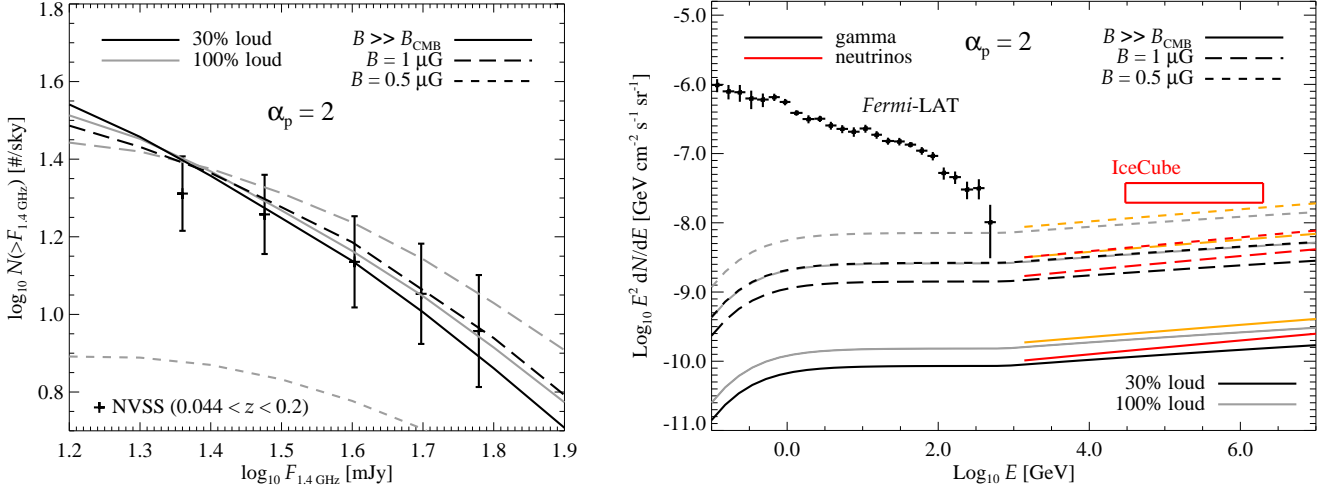


Fig. 3. Same as Figure 3 together with the case of 30% loud clusters for $\alpha_p = 2$ only. The remaining fraction of 70% quiet clusters has been assumed to have $L_\gamma(100 \text{ MeV})$ one order of magnitude lower than for the loud clusters. The 100% loud case is shown with lighter colours (i.e., in grey and orange).

4. Semi-analytical model for the cosmic-ray and intra-cluster-medium distributions

In this Section, we adopt a more sophisticated approach to model the CR and ICM distributions in galaxy clusters, as well as their magnetic field spatial distribution.

4.1. Semi-analytical modelling

For the ICM density distribution, we adopt the phenomenological model of Zandanel et al. (2014a), which is based on gas profiles obtained in X-rays (Croston et al. 2008) and on an observational correlation between gas fraction and mass of the clusters (Sun et al. 2009). This method allows to assign a gas density to any galaxy cluster using its mass only, in such a way that the observed X-ray and Sunyaev-Zel'dovich scaling relations are correctly reproduced.

For the CR spatial and spectral distribution, we adopt the hadronic model proposed in Zandanel et al. (2014b), which extends the semi-analytical model of Pinzke & Pfrommer (2010). The latter provides a scaling of the CR distribution with the cluster mass, while Zandanel et al. (2014b) introduced an effective parameterisation on the CR spatial distribution ρ_{CR} to account for CR transport phenomena. In all the models analysed in this section, we assume the proton spectral shape as in Pinzke & Pfrommer (2010) where a universal CR spectrum is found among the simulated galaxy clusters.

We rely on Equations (3) and (4) with $L_\gamma(M_{500}, z)$ and $L_{1.4}(M_{500}, z)$ calculated by using Equations (2) and (1), with ρ_{ICM} and ρ_{CR} from the Zandanel et al. (2014a,b) models, including redshift evolution.

The cluster population is divided into 50% cool-core and 50% non cool-core clusters (as from observations; see, e.g. Chen et al. 2007) with different parameterisation of the ICM and CR profiles. Cool-core clusters are relaxed objects and, therefore, CRs could stream out of the core creating flat CR profiles. Non cool-core clusters are more turbulent objects which should cause CRs to advect with the gas and create centrally peaked CR profiles. The difference between cool-core and non-cool core clusters is modelled through the parameter $\gamma_{\text{tu}} = \tau_{\text{st}}/\tau_{\text{tu}}$,

i.e., the ratio between the characteristic time scale of streaming and that of turbulence. This parameter ranges from 100, for highly turbulent cluster and centrally peaked CR distributions, to 1, for relaxed clusters and flat distributions as CRs move toward the outskirts (Zandanel et al. 2014b). Here, we assume $\gamma_{\text{tu}} = 3$ and 1 for loud and quiet cool-core clusters, and $\gamma_{\text{tu}} = 60$ and 1 for loud and quiet non cool-clusters, respectively.

The magnetic field is assumed to radially scale as the gas density:

$$B(r) = B_0 \left(\frac{\rho_{\text{ICM}}(r)}{\rho_{\text{ICM}}(0)} \right)^{\alpha_B}, \quad (8)$$

where B_0 is the central magnetic field and $\alpha_B = 0.5$ describes the declining rate of the magnetic field strength toward the cluster outskirts (Dubois & Teyssier 2008; Bonafede et al. 2010; Kuchar & Enßlin 2011, and references therein). In particular, for quiet clusters we adopt a central magnetic field B_0 of $4 \mu\text{G}$ ($7.5 \mu\text{G}$) for non cool-core (cool-core) clusters, while we choose $6 \mu\text{G}$ ($10 \mu\text{G}$), to account for the potential turbulent dynamo in loud objects.

4.2. Results: gamma-ray and neutrino backgrounds

The model in Zandanel et al. (2014b) (ZPP in tables and figures) reproduces the observed radio-to-X-ray and radio-to-Sunyaev-Zel'dovich scaling relations of galaxy clusters and respects current gamma-ray upper limits.⁴ In the left panel of Figure 4, we show the resulting radio counts for a fraction of 20% and 40% loud clusters. We find that the latter case should be considered extreme because hadronic interactions are known not to be uniquely responsible for the observed radio emission in clusters. Table 2 shows the corresponding total gamma-ray and neutrino fluxes.

⁴ The parameters for the corresponding $L_\gamma(100 \text{ MeV})-M_{500}$ scaling relation at $z = 0$ are $P_1 = 21.68$ and $P_2 = 1.62$ for non cool-core clusters, and $P_1 = 22.41$ and $P_2 = 1.57$ for cool-core clusters. This translates in Coma-like and Perseus-like fluxes, for $\alpha_p = 2.2$, of $F(> 100 \text{ MeV}) = 1.6 \times 10^{-9}$ and $F(> 1 \text{ TeV}) = 7.6 \times 10^{-14} \text{ cm}^{-2} \text{ s}^{-1}$, respectively, below the current upper limits.

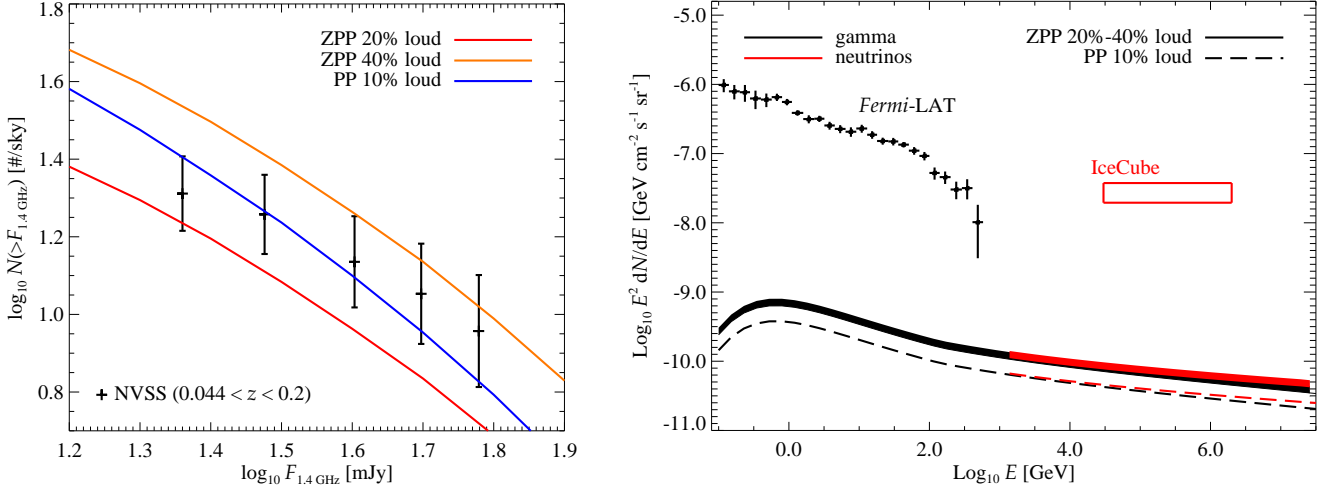


Fig. 4. Radio counts due to synchrotron emission of secondary electrons as from the semi-analytical model of Zandanel et al. (2014b) (ZPP in the plots) on the left, and total gamma-ray and neutrino intensities on the right. For comparison, we plot the *Fermi* (The Fermi LAT collaboration 2014) and IceCube data (Aartsen et al. 2014b) in the panels on the right. The neutrino intensity is meant for all flavours. We show the cases of the model applied to a mass function for 20% and 40% loud clusters, and additionally for 10% loud clusters with parameters as in the Pinzke & Pfrommer (2010) model with a maximum CR proton acceleration efficiency of 15% (PP in the plots). According to this semi-analytical model, galaxy clusters contribute to < 1% to the diffuse gamma-ray and neutrino backgrounds.

Table 2. Total gamma-ray and neutrino fluxes for the semi-analytical model.

Model	I_γ (100 MeV)	I_ν (250 TeV)
ZPP 40%	3.0	1.3
ZPP 20%	2.4	1.0
ZPP 20% $z_2 = 0.6$	2.0	0.9
ZPP 20% $M_{500, \text{lim}} = 10^{13} h^{-1} M_\odot$	6.2	2.3
ZPP 20% <i>Planck</i>	4.2	1.7
PP 10%	1.5	0.6

Note. Total gamma-ray and neutrino flux at 100 MeV and 250 TeV, respectively, for the semi-analytical model in units of 10^{-8} and $10^{-21} \text{ cm}^{-2} \text{ s}^{-1} \text{ GeV}^{-1} \text{ sr}^{-1}$, respectively.

Figure 4 (left panel) also shows the radio counts obtained by adopting a 10% of loud clusters with parameters corresponding to the model in Pinzke & Pfrommer (2010) (PP in tables and figures) with a maximum CR proton acceleration efficiency scaled down to 15% with respect to the originally assumed 50% in order to obey current gamma-ray constraints (Zandanel & Ando 2014; Fermi-LAT Collaboration 2014). For the remaining 90% quiet fraction, the parameters of the previous model are assumed.

The right panel of Figure 4 shows the corresponding total gamma-ray and neutrino intensities compared with the data from *Fermi* and IceCube. We conclude that galaxy clusters contribute to < 1% to the diffuse gamma-ray and neutrino backgrounds.

The results reported in this Section are more realistic than the ones shown in Section 3. However, we underline as the semi-analytical model adopted here is based on the hypothesis that CRs are accelerated at structure formation shocks, while no assumption on the CR sources is made in the phenomenological approach of Section 3.

4.3. Results: dependence on cosmology and lower mass bound

In order to test the robustness of our results, we compute the gamma-ray and neutrino backgrounds in the case of 20% loud clusters, first extending the integration down to smaller masses ($M_{500, \text{lim}} = 10^{13} h^{-1} M_\odot$) and then by adopting the most recent *Planck* results for the cosmological parameters.

The left panel of Figure 5 shows the gamma-ray and neutrino backgrounds for the same case shown in Figure 4 for 20% loud clusters with $M_{500, \text{lim}} = 10^{13.8} h^{-1} M_\odot$ and for the case with $M_{500, \text{lim}} = 10^{13} h^{-1} M_\odot$. In the latter case, the gamma-ray and neutrino diffuse fluxes are significantly higher, while still representing less than 1% of the observational data. At the same time, the radio counts are exactly the same as in Figure 4 as these are due to the higher mass objects.

We additionally show the case of 20% loud clusters, with $M_{500, \text{lim}} = 10^{13.8} h^{-1} M_\odot$, integrated up to $z_2 = 0.6$. As anticipated in Section 2, low redshift objects represent the dominant contribution to the diffuse fluxes, as adopting $z_2 = 0.6$ we obtain 82% of the total flux.

The right panel of Figure 5 shows gamma-ray and neutrino backgrounds for the same case shown in Figure 4 for 20% loud clusters and obtained by adopting the cosmological parameters determined by the *Planck* satellite (Planck Collaboration 2013), i.e., $H_0 = 67.3 \text{ km s}^{-1} \text{ Mpc}^{-1}$, $\Omega_m = 0.32$, $\Omega_\Lambda = 0.68$, and the corresponding mass function. The *Planck* cosmology results in an overall larger number of structures, as clear from Figure 1, therefore increasing both the total radio counts (not shown, but still below the 40% loud case of Figure 4) and the total gamma-ray and neutrino fluxes. As shown in Figure 5, the contribution to the extragalactic gamma-ray and neutrino background is anyhow lower than 1%.

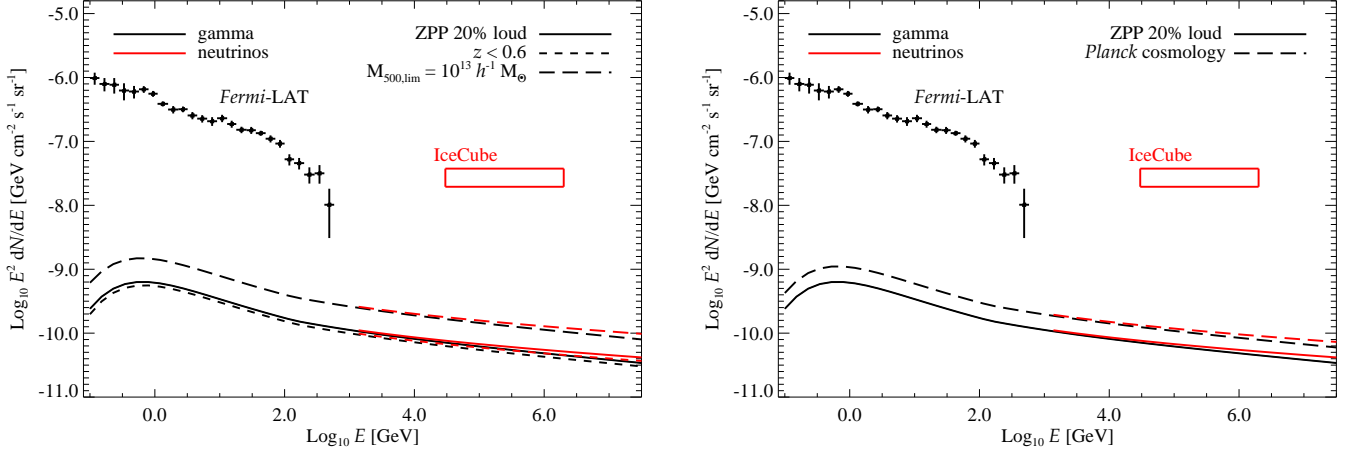


Fig. 5. Same as in the left panel of Figure 4 for 20% loud clusters. The left panel shows the comparison with the previous model with one obtained adopting $z_2 = 0.6$, and one with a lower mass integration limit, of $10^{13} h^{-1} M_{\odot}$. The right panel shows the comparison with the model in Figure 4 and one obtained using the *Planck* cosmological data.

5. Proton-photon interactions in galaxy clusters

Besides interacting with the ICM, relativistic protons in clusters of galaxies can also interact with the ambient photon fields. The two main interaction processes are electron–positron pair production ($p + \gamma \rightarrow p + e^+ + e^-$) and photomeson production ($p + \gamma \rightarrow N + k\pi$, where N indicates a nucleon and k the fact that more than one pion can be produced). In the latter case, both photons and neutrinos are expected, due to the decay of neutral and charged pions, respectively (Kelner & Aharonian 2008). Thus, this is another channel to be investigated in order to assess the contribution of clusters of galaxies to the diffuse neutrino flux observed by IceCube.

The process of photomeson production has a kinematic threshold and takes place when the energy of the photon in the rest frame of the proton exceeds $E_{\text{thr}} \approx 145$ MeV (see e.g., Kelner & Aharonian 2008). The most prominent radiation field in clusters of galaxies is the CMB (e.g., Pinzke et al. 2011), whose photons have a typical energy of $E_{\text{CMB}} \approx 7 \times 10^{-4}$ eV. The threshold energy for a proton to produce a meson is $E_{p,\text{thr}} = E_{\text{thr}}^2 / 2E_{\text{CMB}} \approx 10^{20}$ eV, but in fact also protons with slightly smaller energy can interact with the high energy tail of the black body radiation (Greisen 1966; Zatsepin & Kuz'min 1966). Thus, one can conclude that proton–photon interactions in clusters of galaxies can give a contribution to the high-energy neutrino background only if protons with energy in excess of several 10^{19} eV are present in the ICM.

Accretion shocks around clusters of galaxies have been proposed to be the sites of the acceleration of ultrahigh-energy CRs, the main reason being that their very large (Mpc scale) size would allow the acceleration and confinement of protons of ultrahigh energies (e.g., Norman et al. 1995). An estimate of the maximum energy achievable by protons at cluster accretion shocks can be obtained by equating the acceleration time, computed in the framework of diffusive shock acceleration, to the energy loss time due to proton–photon interactions. Accurate calculations showed that the maximum energy of protons is determined by the energy losses due to electron–positron pair production, and that for the most optimistic assumptions ranges from a few 10^{18} eV to a few 10^{19} eV (Vannoni et al. 2011). Thus, being cooled mainly due to pair production, protons are not expected to produce any appreciable flux of neutrinos through the proton–

photon interaction channel. Heavy nuclei, such as iron, can be accelerated up to $\approx 10^{20}$ eV at cluster accretion shocks (e.g., Allard & Protheroe 2009; Vannoni et al. 2011). However, iron cools mainly due to photodisintegration in a soft photon field and in this case the neutrino yield is much suppressed with respect to the case of photomeson production (Kotera et al. 2009).

Another possible scenario for the production of neutrinos in the ICM would be to assume that clusters contain sources of ultrahigh-energy CRs. This would bring two advantages. First of all, the infrared photon background in the cluster core would be enhanced with respect to the cosmological one due to the contribution from the galaxies in the cluster (Lagache et al. 2005; Pinzke et al. 2011). Secondly, the turbulent magnetic field present within the ICM would partially confine ultrahigh-energy protons, enhancing the probability of interaction. These two facts would increase the expected neutrino flux from proton–photon interactions (e.g., de Marco et al. 2006; Kotera et al. 2009). However, the source of ultrahigh-energy CRs will have to be located in the centre of the cluster, where the infrared photon background is enhanced and the confinement of protons is more effective (due to a larger magnetic field). As pointed out in Kotera et al. (2009), the large gas density in the core of clusters would also enhance the probability of proton–proton interactions, which would dominate the neutrino production below energies of $\approx 10^{18}$ eV. This implies that proton–photon interactions give a negligible contribution to the neutrino flux in the energy domain of the IceCube neutrinos.

6. Contribution to the small-scale anisotropies of the gamma-ray background

Recently, Fermi-LAT Collaboration (2012) analysed the anisotropies in the EGB and found an excess in its angular power spectrum over what it is expected with a completely diffuse source distribution, on multipole ranges $155 \leq \ell \leq 504$ (corresponding to $\lesssim 2^\circ$ angular scales). For the first time, this showed that a major fraction of the EGB is made by discrete sources, and, in fact, Cuoco et al. (2012) pointed out that the measured level of anisotropies is consistent with predictions for gamma-ray blazars (Ando et al. 2007). They also obtained the upper limit on the angular power spectrum

as $C_\ell < 3.3 \times 10^{-18} (\text{cm}^{-2} \text{s}^{-1} \text{sr}^{-1})^2 \text{sr}$ for $155 \leq \ell \leq 504$ and $E = 1\text{--}10 \text{ GeV}$ on other source components, after subtracting the main blazar contribution. Even though the clusters are not the dominant contributors to the isotropic component of the diffuse gamma-ray and neutrino backgrounds (as shown in the previous sections), they may give substantial contributions to the EGB *anisotropies*. In particular, since the number of clusters is relatively fewer than other astrophysical sources, such as star-forming galaxies, the cluster components in the EGB should be more anisotropic. To this end, in this Section, we estimate the cluster contribution to the EGB anisotropies and compare it to the *Fermi* data at sub-degree angular scales.

The angular power spectrum coming from proton-proton interactions in galaxy clusters can be calculated as follows (e.g., Ando et al. 2007):

$$C_\ell = \int \frac{d\chi}{\chi^2} W_\gamma^2(E[1+z], z) P_C\left(k = \frac{\ell}{\chi}, \chi\right), \quad (9)$$

where χ is the comoving distance (we use the same redshift range as in previous sections), $W_\gamma = (1+z)^3 A_\gamma(E[1+z])/4\pi$ is the so-called window function, and $P_C(k, \chi)$ is the power spectrum for the cluster gamma-ray emission. The latter can be divided into one- and two-halo terms, $P_C = P_C^{\text{1h}} + P_C^{\text{2h}}$, which we express as (e.g., Komatsu & Seljak 2002; Ando et al. 2007)

$$P_C^{\text{1h}} = \int dM \frac{dn}{dM} \left[\int 4\pi r^2 dr \rho_{\text{CR}}(r) \rho_{\text{gas}}(r) \frac{\sin(kr)}{kr} \right]^2, \quad (10)$$

$$P_C^{\text{2h}} = \left[\int dM \frac{dn}{dM} b(M, z) \int 4\pi r^2 dr \rho_{\text{CR}}(r) \rho_{\text{gas}}(r) \frac{\sin(kr)}{kr} \right]^2 \times P_{\text{lin}}(k, \chi), \quad (11)$$

respectively, where the radial integration goes up to R_{500} . In the two-halo term, we assume that the linear matter power spectrum $P_{\text{lin}}(k, \chi)$ is related to the cluster power spectrum via the linear bias $b(M, z)$ (Tinker et al. 2010). We find that the one-halo term dominates over the two-halo term at all multipoles ℓ .

In Figure 6, we show the angular power spectrum for the semi-analytical models of Section 4 for 20% and 40% loud clusters integrated in the energy bin from 1 to 10 GeV. We compare with the measurement on the EGB by *Fermi* (Fermi-LAT Collaboration 2012) and upper limits by Cuoco et al. (2012). Note that we compare $C_\ell^{1/2}$ instead of C_ℓ . This is because C_ℓ is a variance, and therefore, if each cluster is twice as bright, then C_ℓ becomes larger by a factor of 4. Therefore, taking the square-root will reflect the correct scaling with respect to the cluster contribution. Our prediction is about one order of magnitude smaller than the *Fermi* upper limit. This means that in scenarios where the total galaxy cluster intensity is much higher with respect to the models of Section 4, as it is potentially realised for some of the simple phenomenological models discussed in Section 3, the angular power spectrum could be a powerful discriminator, as powerful as radio counts.

7. Discussion and conclusions

In this work we estimate the contribution from hadronic proton-proton interactions in galaxy clusters to the total extragalactic gamma-ray and neutrino fluxes while, for the first time, including radio constraints.

We model the cluster population by means of their mass function. Our approach makes use of a phenomenological luminosity-mass relation applied to all clusters, constructed by

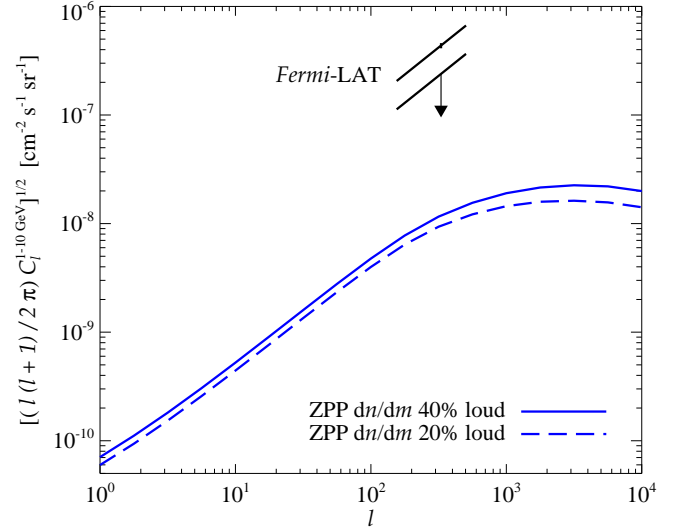


Fig. 6. Gamma-ray angular power spectrum for emission resulting from proton-proton interactions in galaxy clusters in the energy range 1–10 GeV. We show the result for the semi-analytical model of Section 4 for 20% and 40% loud clusters. We plot the EGB anisotropy measured by *Fermi* (Fermi-LAT Collaboration 2012) for comparison, which is explained by unresolved blazars, and the upper limits obtained once the blazar component is subtracted (Cuoco et al. 2012). Note that we plot the square root of $\ell(\ell+1)C_\ell/2\pi$ which implies that the shown quantity is directly proportional to an increase in intensity.

requiring to respect radio counts. We adopt four different proton spectral indices $\alpha_p = 1.5, 2, 2.2$ and 2.4 , and three different magnetic field values $B \gg B_{\text{CMB}}$, $B = 1 \mu\text{G}$ and $B = 0.5 \mu\text{G}$. The latter is meant to be only an illustrative case, as it is in tension with current estimates of magnetic fields in clusters.

Radio observations reveal that not all galaxy clusters host diffuse synchrotron radio emission, with upper limits about an order of magnitude below the loud-state (Brunetti et al. 2009; Cassano et al. 2013). For sake of simplicity, we adopt 100% loud clusters, providing therefore an optimistic estimation. However, we also discuss a case with 30% loud clusters for $\alpha_p = 2$, according to recent estimates on the loud fraction. In our phenomenological model, the redshift evolution is neglected for simplicity and we estimate that this approximation is responsible for results only a factor of 20% below what would be obtained including the redshift evolution.

By requiring to respect all the current constraints from radio counts to gamma-ray upper limits on individual clusters, we show that galaxy clusters can contribute at most up to 10% of the total neutrino background for $\alpha_p = 2$, while contributing much less to the EGB. For $\alpha_p > 2$, in all considered cases, the gamma-ray and neutrino backgrounds are $< 1\%$ of the gamma-ray and neutrino fluxes measured by *Fermi* (Fermi-LAT Collaboration 2010b; The Fermi LAT collaboration 2014) and IceCube (Aartsen et al. 2014b), respectively. Only for the extreme case with $\alpha_p = 1.5$, the neutrino flux is of the same order of magnitude of the IceCube data. Note, however, that such a hard spectral shape is in tension with the most recent IceCube spectral fit of neutrino flux (Aartsen et al. 2014a).

We also adopt a more refined approach which employs a semi-analytical model where the ICM density is constructed

from X-ray observations and the CR spatial and spectral distribution is based on state-of-art hydrodynamic simulations (Zandanel et al. 2014b). In this case, we divide the cluster population into cool-core/non-cool-core and loud/quiet subsamples, as suggested by observations, where the transition from the loud to the quiet state is realised through a change in the CR propagation properties. We find that galaxy clusters contribute to $< 1\%$ to the EGB and to the neutrino flux measured by IceCube. Note that while this semi-analytical model is more realistic than the simplified phenomenological model discussed above, in this case we assume that CRs are accelerated at structure formation shocks, while no assumption on the CR sources was made in the phenomenological approach.

We briefly discuss also the case of proton-photon interactions in galaxy cluster. We found that this channel gives a negligible contribution to the expected neutrino flux in the multi TeV–PeV energy domain.

While galaxy clusters give a subdominant contribution to the EGB, they could substantially contribute to its anisotropy because they are fewer in number than other astrophysical sources and, therefore, are expected to be more anisotropic. For this reason, we compute the angular power spectrum for the considered semi-analytical models and show that the amplitude of the angular fluctuations, represented by $C_\ell^{1/2}$, is about one order of magnitude below the *Fermi* upper limits.

We conclude that there is no realistic scenario in which galaxy clusters can contribute substantially to either the EGB or the extragalactic neutrino flux, being the maximum contribution at most 10% in the simple phenomenological modelling, while $< 1\%$ in most cases and in the more realistic semi-analytical modelling. We also prove that our conclusions are not significantly affected by our assumptions. Our results therefore get into prospective earlier works which resulted to be over-optimistic in estimating the galaxy cluster contribution (e.g., Loeb & Waxman 2000; Murase et al. 2013).

Let us conclude with a few comments on our main assumptions. In our calculations, we neglect a possible cut-off in the CR spectrum at high-energies due to protons that are no longer confined into the cluster, as well as the absorption of high-energy gamma-rays due to interactions with the extragalactic background light. The former implies larger high-energy neutrino fluxes, while the latter implies slightly optimistic gamma-ray fluxes. Additionally, we stress once more how requiring the synchrotron emission from secondary electrons not to overshoot radio counts also results in rather optimistic gamma-ray and neutrino fluxes. This is due to the fact that so-called giant radio halos hosted in merging, non cool-core clusters cannot be explained uniquely by hadronic emission (Brunetti et al. 2012; Zandanel et al. 2014b). Therefore, the secondary emission seems to represent only a fraction of the total observed radio emission.

As a final note on the semi-analytical modelling, we underline that the transition from the loud to the quiet state in the galaxy cluster population is not realised in the *classical* hadronic model, meaning that it predicts all clusters should have the same level of secondary emission. This is in clear tension with observations and represents one of the problems of the hadronic scenario (see Enßlin et al. 2011 for a discussion). The only mechanism that has been proposed so far to solve this problem is that of varying CR propagation properties (see, e.g., Wiener et al. 2013), also adopted in our semi-analytical approach through the Zandanel et al. (2014b) model. We note, however, that it is still under debate whether the conditions for CR diffusion can be realised in the ICM or not. In the worst case scenario, the sec-

ondary electrons produced in proton-proton collisions in clusters would only be seed for subsequent turbulent re-acceleration (see, e.g., Brunetti & Lazarian 2011; Brunetti et al. 2012). This would imply a much lower secondary emission, only at the level of the quiet-state. If this will turn out to be the case, the total gamma-ray and neutrino fluxes from galaxy clusters should be even lower than what we estimated here.

Acknowledgements. We thank Denis Allard, Rossella Cassano and Kohta Murase for useful discussions. This work was supported by the Netherlands Organization for Scientific Research (NWO) through a Vidi grant (SA, IT and FZ) and a PHC Van Gogh grant (SG).

References

- Aartsen, M. et al. 2013, *Phys.Rev.Lett.*, 111, 021103
Aartsen, M. et al. 2014a, *ArXiv:1410.1749*
Aartsen, M. et al. 2014b, *Phys.Rev.Lett.*, 113, 101101
Abdo, A. A., Ackermann, M., Ajello, M., et al. 2010, *ApJ*, 720, 435
Ackermann, M. et al. 2012, *Astrophys.J.*, 755, 164
Ahlers, M. & Murase, K. 2014, *Phys.Rev.*, D90, 023010
Allard, D. & Protheroe, R. J. 2009, *A&A*, 502, 803
Anchordoqui, L. A., Barger, V., Cholis, I., et al. 2014a, *Journal of High Energy Astrophysics*, 1-2, 1
Anchordoqui, L. A., Goldberg, H., Halzen, F., & Weiler, T. J. 2004, *Phys.Lett.*, B600, 202
Anchordoqui, L. A., Goldberg, H., Paul, T. C., da Silva, L. H. M., & Vlcek, B. J. 2014b, *ArXiv:1410.0348*
Anchordoqui, L. A., Paul, T. C., da Silva, L. H. M., Torres, D. F., & Vlcek, B. J. 2014c, *Phys.Rev.*, D89, 127304
Ando, S., Komatsu, E., Narumoto, T., & Totani, T. 2007, *Phys.Rev.*, D75, 063519
Ando, S. & Nagai, D. 2008, *MMRAS.*, 385, 2243
Ando, S. & Nagai, D. 2012, *JCAP*, 7, 17
Berezinsky, V. S., Blasi, P., & Ptuskin, V. S. 1997, *ApJ*, 487, 529
Blasi, P. & Colafrancesco, S. 1999, *Astroparticle Physics*, 12, 169
Blasi, P., Gabici, S., & Brunetti, G. 2007, *International Journal of Modern Physics A*, 22, 681
Bonafede, A., Feretti, L., Murgia, M., et al. 2010, *A&A*, 513, A30+
Bonafede, A., Vazza, F., Brügggen, M., et al. 2013, *MNRAS*
Brunetti, G., Blasi, P., Reimer, O., et al. 2012, *MNRAS*, 426, 956
Brunetti, G., Cassano, R., Dolag, K., & Setti, G. 2009, *A&A*, 507, 661
Brunetti, G. & Jones, T. W. 2014, *International Journal of Modern Physics D*, 23, 30007
Brunetti, G. & Lazarian, A. 2011, *MNRAS*, 410, 127
Carilli, C. L. & Taylor, G. B. 2002, *ARA&A*, 40, 319
Cassano, R., Brunetti, G., Norris, R. P., et al. 2012, *A&A*, 548, A100
Cassano, R., Brunetti, G., Röttgering, H. J. A., & Brügggen, M. 2010, *A&A*, 509, A68
Cassano, R., Etori, S., Brunetti, G., et al. 2013, *ApJ*, 777, 141
Chang, X.-C. & Wang, X.-Y. 2014, *ApJ*, 793, 131
Chen, Y., Reiprich, T. H., Böhringer, H., Ikebe, Y., & Zhang, Y.-Y. 2007, *A&A*, 466, 805
Clarke, T. E. 2004, *Journal of Korean Astronomical Society*, 37, 337
Croston, J. H., Pratt, G. W., Böhringer, H., et al. 2008, *A&A*, 487, 431
Cuoco, A., Komatsu, E., & Siegal-Gaskins, J. M. 2012, *Phys.Rev.D*, 86, 063004
de Marco, D., Hansen, P., Stanev, T., & Blasi, P. 2006, *Phys. Rev. D*, 73, 043004
Dennison, B. 1980, *ApJL*, 239, L93
Dermer, C. D. 2007, *AIP Conf.Proc.*, 921, 122
Di Mauro, M., Calore, F., Donato, F., Ajello, M., & Latronico, L. 2014a, *ApJ*, 780, 161
Di Mauro, M., Donato, F., Lamanna, G., Sanchez, D. A., & Serpico, P. D. 2014b, *ApJ*, 786, 129
Domínguez, A., Primack, J. R., Rosario, D. J., et al. 2011, *MNRAS*, 410, 2556
Dubois, Y. & Teyssier, R. 2008, *A&A*, 482, L13
Enßlin, T., Pfrommer, C., Miniati, F., & Subramanian, K. 2011, *A&A*, 527, A99+
Esmaili, A., Kang, S. K., & Serpico, P. D. 2014, *ArXiv:1410.5979*
Esmaili, A. & Serpico, P. D. 2013, *JCAP*, 1311, 054
Feldstein, B., Kusenko, A., Matsumoto, S., & Yanagida, T. T. 2013, *Phys.Rev.*, D88, 015004
Feretti, L., Giovannini, G., Govoni, F., & Murgia, M. 2012, *A&Ar*, 20, 54
Fermi-LAT Collaboration. 2010a, *ApJL*, 717, L71
Fermi-LAT Collaboration. 2010b, *Physical Review Letters*, 104, 101101
Fermi-LAT Collaboration. 2012, *Phys.Rev.D*, 85, 083007
Fermi-LAT Collaboration. 2014, *ApJ*, 787, 18
Fichtel, C. E., Hartman, R. C., Kniffen, D. A., et al. 1977, *ApJL*, 217, L9

- Fornasa, M., Zavala, J., Sánchez-Conde, M. A., et al. 2013, *MNRAS*, 429, 1529
- Fox, D., Kashiyama, K., & Mszars, P. 2013, *Astrophys.J.*, 774, 74
- Gabici, S. & Blasi, P. 2003, *Astroparticle Physics*, 19, 679
- Giovannini, G., Tordi, M., & Feretti, L. 1999, *New A*, 4, 141
- Greisen, K. 1966, *Physical Review Letters*, 16, 748
- Griffin, R. D., Dai, X., & Kochanek, C. S. 2014, *ApJL*, 795, L21
- He, H.-N., Wang, T., Fan, Y.-Z., Liu, S.-M., & Wei, D.-M. 2013, *Phys.Rev.*, D87, 063011
- HESS Collaboration. 2009a, *A&A*, 502, 437
- HESS Collaboration. 2009b, *A&A*, 495, 27
- Huber, B., Tchernin, C., Eckert, D., et al. 2013, *A&A*, 560, A64
- Joshi, J. C., Winter, W., & Gupta, N. 2014, *MNRAS*, 439, 3414
- Kale, R., Venturi, T., Giacintucci, S., et al. 2013, *A&A*, 557, A99
- Kashiyama, K. & Meszaros, P. 2014, *Astrophys.J.*, 790, L14
- Katz, B., Waxman, E., Thompson, T., & Loeb, A. 2013, *ArXiv:1311.0287*
- Kelner, S. R. & Aharonian, F. A. 2008, *Physical Review D*, 78, 034013
- Kelner, S. R., Aharonian, F. A., & Bugayov, V. V. 2006, *Phys. Rev. D*, 74, 034018
- Keshet, U., Waxman, E., Loeb, A., Springel, V., & Hernquist, L. 2003, *ApJ*, 585, 128
- Komatsu, E. & Seljak, U. 2002, *Mon.Not.Roy.Astron.Soc.*, 336, 1256
- Komatsu, E., Smith, K. M., Dunkley, J., et al. 2011, *ApJS*, 192, 18
- Kotera, K., Allard, D., Murase, K., et al. 2009, *ApJ*, 707, 370
- Kuchar, P. & EnBlin, T. A. 2011, *A&A*, 529, A13+
- Kushnir, D. & Waxman, E. 2009, *JCAP*, 8, 2
- Lacki, B. C., Thompson, T. A., Quataert, E., Loeb, A., & Waxman, E. 2011, *Astrophys.J.*, 734, 107
- Lagache, G., Puget, J.-L., & Dole, H. 2005, *ARA&A*, 43, 727
- Liu, R.-Y., Wang, X.-Y., Inoue, S., Crocker, R., & Aharonian, F. 2014, *Phys.Rev.*, D89, 083004
- Loeb, A. & Waxman, E. 2000, *Nature*, 405, 156
- Loeb, A. & Waxman, E. 2006, *JCAP*, 0605, 003
- MAGIC Collaboration. 2010, *ApJ*, 710, 634
- MAGIC Collaboration. 2012, *A&A*, 541, A99
- Miniati, F., Ryu, D., Kang, H., & Jones, T. W. 2001, *ApJ*, 559, 59
- Murase, K., Ahlers, M., & Lacki, B. C. 2013, *Phys.Rev.*, D88, 121301
- Murase, K., Ahlers, M., & Lacki, B. C. 2013, *Physical Review D*, 88, 121301
- Murase, K. & Beacom, J. F. 2013, *JCAP*, 2, 28
- Murase, K., Inoue, S., & Nagataki, S. 2008, *ApJl*, 689, L105
- Murase, K., Inoue, Y., & Dermer, C. D. 2014, *Phys.Rev.*, D90, 023007
- Murase, K. & Ioka, K. 2013, *Phys.Rev.Lett.*, 111, 121102
- Murray, S. G., Power, C., & Robotham, A. S. G. 2013, *Astronomy and Computing*, 3, 23
- Norman, C. A., Melrose, D. B., & Achterberg, A. 1995, *ApJ*, 454, 60
- Padovani, P. & Resconi, E. 2014, *MNRAS*, 443, 474
- Pfrommer, C. 2008, *MNRAS*, 385, 1242
- Pfrommer, C. & EnBlin, T. A. 2004, *A&A*, 413, 17
- Pfrommer, C., EnBlin, T. A., & Springel, V. 2008, *MNRAS*, 385, 1211
- Pinzke, A. & Pfrommer, C. 2010, *MNRAS*, 409, 449
- Pinzke, A., Pfrommer, C., & Bergström, L. 2011, *Phys. Rev. D.*, 84, 123509
- Planck Collaboration. 2013, *ArXiv:1303.5076*
- Prokhorov, D. A. & Churazov, E. M. 2014, *A&A*, 567, A93
- Razzaque, S. 2013, *Phys.Rev.*, D88, 081302
- Reiprich, T. H. & Böhringer, H. 2002, *ApJ*, 567, 716
- Riebe, K., Partl, A. M., Enke, H., et al. 2013, *Astronomische Nachrichten*, 334, 691
- Siegal-Gaskins, J. M., Reesman, R., Pavlidou, V., Profumo, S., & Walker, T. P. 2011, *MNRAS*, 415, 1074
- Sreekumar, P., Bertsch, D. L., Dingus, B. L., et al. 1998, *ApJ*, 494, 523
- Stecker, F. W. 2013, *Phys.Rev.*, D88, 047301
- Stecker, F. W. & Venters, T. M. 2011, *Astrophys.J.*, 736, 40
- Strong, A. W., Moskalenko, I. V., & Reimer, O. 2004, *ApJ*, 613, 956
- Sun, M., Voit, G. M., Donahue, M., et al. 2009, *ApJ*, 693, 1142
- Tamborra, I., Ando, S., & Murase, K. 2014, *JCAP*, 9, 43
- Taylor, A. M., Gabici, S., & Aharonian, F. 2014, *Phys.Rev.*, D89, 103003
- The Fermi LAT collaboration. 2014, *ArXiv:1410.3696*
- Tinker, J., Kravtsov, A. V., Klypin, A., et al. 2008, *ApJ*, 688, 709
- Tinker, J. L., Robertson, B. E., Kravtsov, A. V., et al. 2010, *ApJ*, 724, 878
- Vannoni, G., Aharonian, F. A., Gabici, S., Kelner, S. R., & Prosekin, A. 2011, *A&A*, 536, A56
- Vazza, F. & Brügggen, M. 2014, *MNRAS*, 437, 2291
- Venturi, T., Giacintucci, S., Brunetti, G., et al. 2007, *A&A*, 463, 937
- Venturi, T., Giacintucci, S., Dallacasa, D., et al. 2008, *A&A*, 484, 327
- VERITAS Collaboration. 2012, *ApJ*, 757, 123
- Vogt, C. & EnBlin, T. A. 2005, *A&A*, 434, 67
- Voit, G. M. 2005, *Reviews of Modern Physics*, 77, 207
- Völk, H. J., Aharonian, F. A., & Breitschwerdt, D. 1996, *Space Science Reviews*, 75, 279
- Waxman, E. 2013, *ArXiv:1312.0558*
- Wiener, J., Oh, S. P., & Guo, F. 2013, *MNRAS*, 434, 2209
- Zandanel, F. & Ando, S. 2014, *MNRAS*, 440, 663
- Zandanel, F., Pfrommer, C., & Prada, F. 2014a, *MNRAS*, 438, 116
- Zandanel, F., Pfrommer, C., & Prada, F. 2014b, *MNRAS*, 438, 124
- Zatsepin, G. T. & Kuz'min, V. A. 1966, *Soviet Journal of Experimental and Theoretical Physics Letters*, 4, 78